Dynamic Stark shift and alignment-to-orientation conversion

Matthew C. Kuntz,* Robert C. Hilborn,† and Alison M. Spencer
Department of Physics, Amherst College, Amherst, Massachusetts 01002-5000
(Received 6 September 2001; published 15 January 2002)

We have observed alignment-to-orientation conversion in the $(5d6p)\ ^1P$ state of atomic barium due to the combined effects of a static Zeeman shift and a dynamic Stark shift associated with the electric field of a pulsed laser beam. The measurements yield a value for the frequency-dependent tensor polarizability of the state in reasonable agreement with a simple perturbation theory calculation. With a tunable laser producing the dynamic Stark shift, we can both enhance the magnitude of the effect by tuning close to a resonance and reverse the sign of the orientation by tuning above or below the resonance. This method of producing an oriented atomic state is quite general, and with easily available field strengths can produce large orientations.

DOI: 10.1103/PhysRevA.65.023411 PACS number(s): 32.60.+i, 42.50.Gy, 32.80.Bx

I. INTRODUCTION

The dynamic (or ac or optical) Stark shift [1,2] has played an important role in many recent advances in atomic physics including precision measurements of atomic polarizabilities [3]. The dynamic Stark shift also contributes to the light force on atoms, which can be used both for the determination of atomic polarizabilities [4] and for laser cooling of atoms and molecules [5]. Furthermore, the dynamic polarizability is important in understanding atom diffraction by standing light waves and the resulting possibilities for sensitive interferometry [6,7]. Under appropriate conditions the dynamic Stark shift can have a major effect on the stability of atoms in intense laser fields [8]. At a more fundamental level, the dynamic Stark shift can be used for quantum nondemolition measurements of photon number states [9,10].

Most of the work cited in the preceding paragraph has concentrated on the energy-level shifts caused by the dynamic Stark effect. Since most atomic states have an anisotropic polarizability (different polarizabilities for the electric field parallel or perpendicular to the atomic angular momentum), different magnetic quantum number states will have different Stark shifts. These differential (or ''tensor'') dynamic Stark shifts can have a significant effect on the evolution of coherences among the atomic sublevels, thereby affecting the polarization of the light emitted (or absorbed) by those states. Such tensor ''light shifts'' were first observed within the context of optical pumping [11]. More recently several authors [12,13] have proposed using the anisotropic light shift to align and possibly to trap molecules.

The coherence properties of atomic states can be described in several ways. One simple method makes use of the notions of ''orientation'' and ''alignment'' of the states. A quantum state is said to be oriented along some axis if the magnetic sublevels associated with m and $-m$ have different populations. In a similar fashion, we say that the state is aligned (with respect to that axis) if the sublevels with different values of $|m|$ have different populations [14]. We note that some authors (for example, Ref. [15], p. 106) define a state to be oriented if some odd multipole moment of the state is not equal to zero and to be aligned if some even multipole is not equal to zero. In this paper, we will use the definitions involving m sublevel populations.

More formally, we can relate the degree of orientation of a state of definite angular momentum to the expectation values of various angular momentum operators. For orientation we have [15–17]

$$O_{1^-}=\frac{\langle \hat{J}_z\rangle}{\hbar J\langle J+1\rangle}, \tag{1}$$

where J is the total angular momentum quantum number. The degree of alignment is specified by the following three quantities:

$$A_0=\frac{\langle 3\hat{J}_z^2-\hat{J}^2\rangle}{\hbar^2 J(J+1)},$$

$$A_{1^+}=\frac{\langle \hat{J}_x\hat{J}_z+\hat{J}_z\hat{J}_x\rangle}{\hbar^2 J(J+1)},$$

$$A_{2^+}=\frac{\langle \hat{J}_x^2-\hat{J}_y^2\rangle}{\hbar^2 J(J+1)}. \tag{2}$$

For a state of definite angular momentum, this description is equivalent to an alternative (and more general) description of the coefficients used to expand the atomic density matrix in terms of irreducible tensor operators [15], the so-called state multipoles or polarization moments.

Since most interatomic interactions depend on the orientation and alignment of the atomic angular momenta [18] and since many experiments, such as searches for time-reversal symmetry violations [19] in atoms, use oriented atomic and molecular states, there is considerable interest in producing oriented or aligned atoms and molecules.

Any anisotropic interaction, such as excitation with linearly polarized light, can produce an aligned atomic state. We are interested in mechanisms that can convert an aligned state into an oriented state. For example, Lombardi [20]

*Present address: WorldStreet Corporation, Boston, MA.
†Email address: rchilborn@amherst.edu

demonstrated circular polarization emission from a radio frequency discharge in helium in a static magnetic field. The electric field of the discharge in combination with the static magnetic field produced the alignment-to-orientation conversion (AOC). Cohen-Tannoudji and Dupont-Roc [21] observed alignment-to-orientation conversion in an optical pumping experiment when the direction of linear polarization of the pumping beam is neither orthogonal nor parallel to the direction of propagation of an unpolarized (nonresonant) dynamic Stark shift beam. The influence of the dynamic Stark shift on the appearance of orientation in atomic ground states has been considered both experimentally and theoretically [22,23] in the context of optical pumping. More recently, static orthogonal electric and magnetic fields were used to produce AOC in atomic barium and atomic cesium [24].

Budker *et al.* [25] showed that alignment-to-orientation conversion due to the dynamic Stark effect plays a significant role in the nonlinear magneto-optical effect, a technique proposed to provide ultrasensitive magnetometry. In fact, for the optical frequencies and light intensities at which nonlinear magneto-optical rotation shows the highest sensitivity to magnetic fields, AOC due to the combination of the static magnetic field and the optical electric field is the primary physical mechanism for optical rotation.

In this paper, we shall demonstrate that an optical electric field can produce an anisotropic dynamic Stark shift and strong alignment-to-orientation conversion in atomic excited states, producing sizable orientations with modest-intensity far-off-resonance light. Since the dynamic Stark shift is frequency dependent, we can enhance the size of the effect by many orders of magnitude by tuning the optical frequency close to an atomic resonance. The results presented here are a demonstration of the off-resonance effect in the evolution of an excited atomic energy level. Other mechanisms for alignment-to-orientation conversion have been discussed in Refs. [24,26,27].

Finally, we mention in passing that the dynamics of atomic states in the presence of orthogonal electric and magnetic fields has been of interest in the study of quantum chaos [28]. A corresponding classical system [29] also exhibits interesting nonlinear dynamics. A recent paper [30] has demonstrated that the dynamic (optical) Stark shift in combination with a static magnetic field can be used to manipulate electron spin orientation on a femtosecond time scale in semiconductors.

II. THEORY

Figure 1 depicts the experimental situation we wish to describe. A static magnetic field in the z direction is applied to the atomic vapor. The atoms are excited by a laser pulse whose frequency is tuned to be in resonance with the ground state to excited state transition. The excitation light at 350 nm propagates in the y direction and is linearly polarized along the x direction. The Stark shift light at 532 nm is also linearly polarized along x. The detector polarizers are set to transmit circularly polarized light emitted along the z direction. A simplified energy-level diagram for atomic barium is shown in Fig. 2.

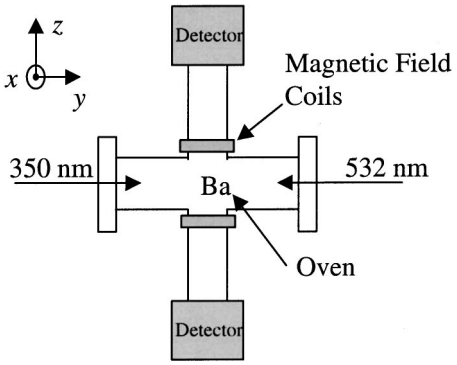

FIG. 1. A schematic diagram of the apparatus. Ba vapor is produced in an evacuated oven. A static magnetic field is applied along the z direction. Both laser beams are linearly polarized along the x direction. Each detector system consists of a bandpass filter at 350 nm, circular polarizers, and a photomultiplier tube.

The theory of the dynamic Stark shift is well known [2,31,32]. The effect on atomic energy levels can be expressed in terms of an effective Hamiltonian [33,34] acting within a particular J state manifold. For an electric field in the x direction, the case of interest in our experiments, we have

$$\hat{H}_{\text{eff}} = -\frac{1}{2}\alpha_0(\omega)E_x^2(t)\hat{I} - \frac{1}{2}\alpha_2(\omega)E_x^2(t)\frac{3\hat{J}_x^2 - \hat{J}^2}{J(2J-1)\hbar^2}, \tag{3}$$

where α_0 is the so-called scalar polarizability and α_2 is the tensor polarizability. $E_x(t)$ is the slowly varying envelope of the electric-field amplitude. Since the scalar polarizability term shifts all of the magnetic sublevels equally and since the shifts are small compared to the excitation laser bandwidth, we will ignore that part of the Stark shift in the remainder of our discussion.

Using second-order perturbation theory, we can express the tensor polarizability of the J state with energy E as

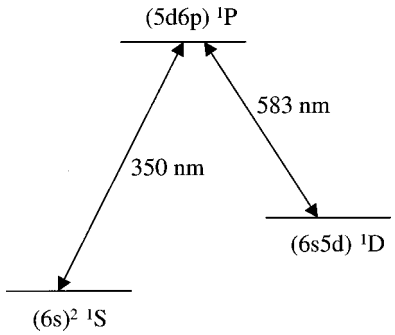

FIG. 2. A simplified energy-level diagram for atomic barium. The atoms are excited with 350 nm light. The circular polarization of the fluorescence at 350 nm is detected.

$$\alpha_2(\omega)=\left[\frac{10J(2J-1)}{3(2J+3)(J+1)(2J+1)}\right]^{1/2} \times \sum_{E'\neq E} |(\Psi'\|\hat{d}\|\Psi)|^2\left[\frac{1}{E-E'+\hbar\omega}+\frac{1}{E-E'-\hbar\omega}\right] \times(-1)^{J+J'+1}\begin{Bmatrix} J & J' & 1 \\ 1 & 2 & J \end{Bmatrix}, \quad (4)$$

where $\hat{d}$ is the operator for the transition electric dipole moment along the external electric-field direction, and the quantity in curly brackets is the standard $6j$ symbol. The vertical double bars indicate the reduced matrix element for the dipole operator. The sum is over all bound and continuum states. Equation (4) reduces to the expression [33] for the static field tensor polarizability in the limit $\omega\rightarrow 0$. Equation (4) is valid as long as the Stark beam detuning is large compared to the atomic linewidth. [In our experiment the detuning was always larger than the Doppler width (about 1.5 GHz), which is turn is much larger than the natural linewidth (about 83 MHz [35]).]

If the external electric-field amplitude were constant in time, the atomic state evolution would be the same as that observed in the static field case, with the static electric-field magnitude replaced by the rms value of the oscillating field [29], weighted by the appropriately changed energy denominators as indicated in Eq. (4). In our experiment, however, the Stark shift field is pulsed. Hence, we must resort to a numerical integration of the Schrödinger equation or, equivalently, to integration of the time-evolution equations for the multipole moments of the density matrix for the excited atom. The general time-evolution equations for the polarization moments are given in Refs. [36] and [37].

The analysis is considerably simplified for a $J=1$ excited state decaying to a $J=0$ lower state, the case for our experiment. In that case we need to find the evolution of only the $m=+1$ and -1 sublevels of the excited state since we are detecting circularly polarized light. We write the state function for the excited state as a (time-dependent) linear superposition of the $m=+1$ and -1 states:

$$|\Psi\rangle=c_+(t)|m=+1\rangle+c_-|m=-1\rangle. \quad (5)$$

Using the Stark shift Hamiltonian given in Eq. (3) and the usual $-\vec{\mu}\cdot\vec{B}$ Hamiltonian for the interaction with the static magnetic field, we find that the time-evolution equations for the state coefficients can be written as

$$i\hbar\dot{c}_+=[p(t)+\beta]c_+-3p(t)c_--ic_+\gamma/2+f(t),$$

$$i\hbar\dot{c}_-=[p(t)-\beta]c_--3p(t)c_+-ic_-\gamma/2-f(t), \quad (6)$$

where $\beta=g_J\mu_B B_z/h$ and $p(t)=\alpha_2(\omega)E_x^2(t)/(4h)$. As usual, g_J is the gyromagnetic ratio for the state, and μ_B is the Bohr magneton. γ is the decay rate of the excited-state population, and $f(t)$ models the laser excitation of the excited state. The relative sign difference in the $f(t)$ terms comes from the appropriate Clebsch-Gordan coefficients for light linearly polarized in the x direction. Given a model for the time dependence of the Stark pulse and the excitation pulse, we can solve Eqs. (6) numerically for the state coefficients starting with $c_+(0)=c_-(0)=0$.

The asymmetry in the circular polarization of the detected fluorescence, $\mathcal{A}_{\rm CP}(t)$, is defined in terms of the intensities of left-circularly-polarized light ($I_{\rm LCP}$) and right-circularly-polarized light ($I_{\rm RCP}$) emitted along the positive z direction:

$$\mathcal{A}_{\rm CP}(t)=\frac{I_{\rm LCP}-I_{\rm RCP}}{I_{\rm LCP}+I_{\rm RCP}}. \quad (7)$$

For a $J=1$ to 0 transition (the case at hand), the difference in intensities for left- and right-circularly-polarized emission is directly proportional to the orientation of the excited state [15,29]. (For more general states, one would need to measure the full set of Stokes parameters of the emitted light to determine the orientation [15].) The circular polarization asymmetry of the excited-state fluorescence in a transition to a $J=0$ lower state is then found from

$$\mathcal{A}_{\rm CP}(t)=\frac{|c_+(t)|^2-|c_-(t)|^2}{|c_+(t)|^2+|c_-(t)|^2}. \quad (8)$$

To explore some of the features of these calculations, we have plotted in Fig. 3 $\mathcal{A}_{\rm CP}(t)$ for two different Stark pulse energies under conditions similar to the experiment described below. The static magnetic field is fixed at 18 G. Also shown are the excitation pulse and the Stark pulse for conditions similar to those used in the experiment. Time is in units of the excited-state mean lifetime. We note several features. First, the orientation (proportional to $\mathcal{A}_{\rm CP}$) is zero until the Stark pulse turns on since for our experimental conditions both the Stark field and the magnetic field must be present to achieve alignment-to-orientation conversion. Second, the orientation stops evolving once the Stark shift pulse is over. The third point to note is that for higher Stark pulse energies the orientation can change sign during its evolution.

Figure 4 shows a sequence of plots indicating the time evolution of the angular momentum distribution described by our calculations. This distribution is calculated as follows [38–41]: To find the probability that the atom's angular momentum vector points in a direction specified by the usual spherical coordinate system angles ϕ and θ, we use the rotation operators [14] $R(\phi,\theta,0)$ to rotate the quantization axis for the density matrix to lie along the direction specified by ϕ and θ. We then take the $(J,m=J)$ matrix element of the rotated density operator $\hat{\rho}$. More formally, we write the angular momentum distribution $\rho(\theta,\phi)$ as

$$\rho(\theta,\phi)=\langle J,m=J|R^{-1}(\phi,\theta,0)\hat{\rho}R(\phi,\theta,0)|J,m=J\rangle. \quad (9)$$

This formalism is closely related to the so-called coherent representation [42,43] of atomic angular momentum states.

Let us explore how the plotted distribution represents the quantum-mechanical expectation values. For example, for a $J=1$ state, with the state coefficients given by

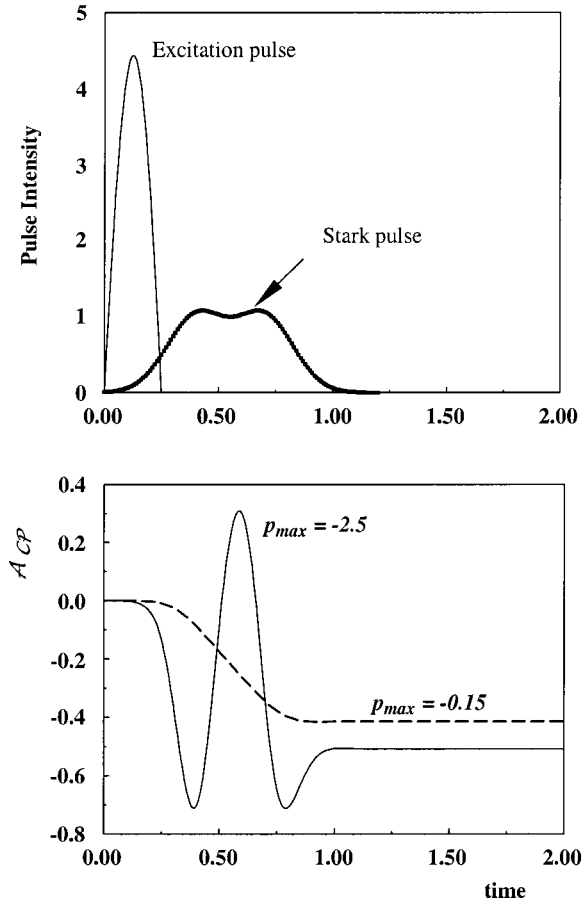

FIG. 3. The top frame shows the excitation pulse and the Stark pulse as functions of time. (The relative heights of the pulses are not significant.) Time is in units of the excited-state mean lifetime. The lower frame indicates the circular polarization asymmetry ($\mathcal{A}_{\mathrm{CP}}$) for two different Stark pulse intensities. The static magnetic field B is 18 G. $p_{\max}$ is proportional to the maximum intensity of the Stark pulse multiplied by the tensor polarizability.

$$c_{+1}=\frac{1}{\sqrt{2}},$$

$$c_{-1}=-\frac{1}{\sqrt{2}}, \tag{10}$$

$$c_0=0$$

(which corresponds to the initial state excited by light linearly polarized along x), the angular momentum expectation values are

$$\langle J_x\rangle=\langle J_y\rangle=\langle J_z\rangle=0,$$

$$\langle J_y^2\rangle=\langle J_z^2\rangle=\hbar^2, \tag{11}$$

$$\langle J_x^2\rangle=0.$$

Equation (9) applied to this situation gives a doughnutlike distribution as shown in the upper left part of Fig. 4. If we

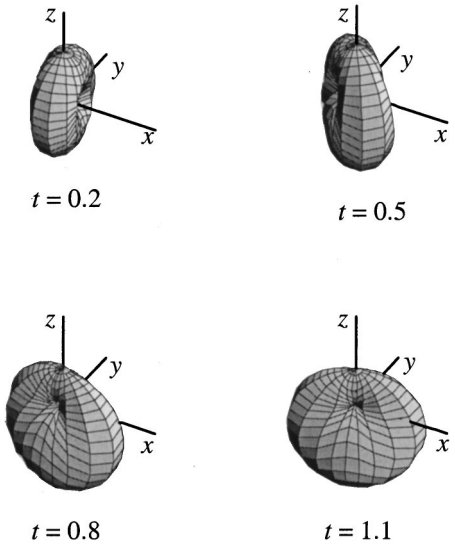

FIG. 4. Three-dimensional plot of the angular momentum distribution function Eq. (9) for $B=18$ G, $p_{\max}=-0.15$. The excitation pulse and Stark pulse timing is illustrated in the upper part of Fig. 3. Time is in units of the excited-state lifetime. The excitation pulse and the Stark pulse are linearly polarized along x. The magnetic field is along z. At $t=0.2$, the initially aligned distribution has rotated slightly under the action of the static magnetic field. The Stark pulse begins at about $t=0.4$. By $t=0.8$, the distribution shows orientation along $-z$.

are at the origin and look along the x axis, we see zero distribution in that direction consistent with the first and last lines of Eq. (11). Along the y and z axes, we see a distribution symmetric about the origin consistent with the first line of Eq. (11), and with equal spread along y and z, consistent with the second line. Since the density matrix for the $J=1$ state can be expressed in terms of expectation values for the angular momentum operators [15], including terms such as $\langle J_xJ_y\rangle$, the density matrix can be reconstructed directly from a plot such as that shown in Fig. 4.

Figure 4 shows that the distribution starts out as pure alignment with equal weights along $+z$ and $-z$. Under the action of the magnetic field alone, the distribution rotates, as is well known, about the z axis. When the Stark pulse turns on significantly (at about $t=0.5$ in Fig. 4), the torque due to the Stark field interacting with the anisotropic induced electric dipole moment causes the angular momentum to evolve toward either $+z$ or $-z$ depending on the sign of the tensor polarizability. By $t=0.8$, the distribution shows a clear preference for the $-z$ direction, indicating a net orientation along the $-z$ direction. If the magnetic field is not present, the initial angular momenta remain perpendicular to the Stark field (along x) and there is no electric-field-induced torque since in that case the induced electric dipole moment and the electric field are parallel. The maximum orientation achieved for the conditions illustrated in Fig. 4 is about -0.4.

The theory outlined above indicates that the observed circular polarization asymmetry depends sensitively on the timing between the excitation pulse and the Stark pulse. To explore that feature, we have calculated $\mathcal{A}_{\mathrm{CP}}(t)$ with a delay of

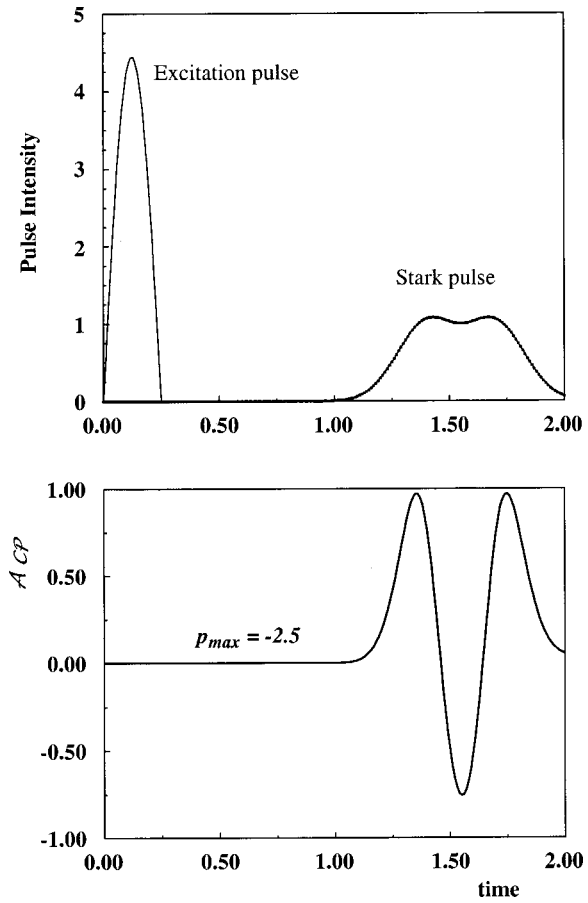

FIG. 5. The circular polarization asymmetry plotted as a function of time with a delay of about 12 ns between the excitation pulse and the Stark pulse. Time is in units of the excited-state mean lifetime.

about 12 ns between the excitation pulse and the Stark pulse as illustrated in the upper part of Fig. 5. The lower part of Fig. 5 shows $\mathcal{A}_{\mathrm{CP}}$ as a function of time. Note again that $\mathcal{A}_{\mathrm{CP}}=0$ until the Stark pulse begins. In Sec. IV, we will discuss the corresponding experimental results.

In our analysis, we have ignored the hyperfine structure of the odd-atomic-number barium isotopes ^{135}Ba with 6.6% natural abundance and ^{137}Ba with 11.3% natural abundance. Detailed calculations for the static electric-field alignment-to-orientation conversion [24] have shown that the odd isotopes contribute only a few percent to the observed alignment-to-orientation conversion due to cancellation of effects from the various hyperfine levels. An analogous cancellation was observed in an AOC experiment in atomic sodium [44]. In the experiment described below, we integrate the circular polarization intensities over time; so the calculated signal is also integrated over time to compare with the experimental results.

III. EXPERIMENT

The experimental apparatus is essentially identical to that used in the static field experiments on atomic barium [24], but we include here a brief description for the sake of completeness. (See Figs. 1 and 2.) Barium atoms are vaporized in an evacuated oven whose central portion is heated to about 600 °C. A helium buffer gas at a pressure of about 0.1 Torr prevents the barium atoms from migrating to the cooled windows of the oven. The barium atoms are excited to the $(5d6p)\ ^1P$ state by pulses of 350 nm light produced by frequency-doubling the output of a Continuum TDL-60 tunable dye laser. The dye laser is pumped by the 532 nm output of a frequency-doubled Continuum 660B neodymium-doped yttrium aluminum garnet (Nd: YAG) laser. The laser system operates at a pulse repetition rate of 20 Hz. The 350 nm pulses are about 3 ns long, short compared to the 12 ns radiative lifetime of the excited state. The 350 nm light is linearly polarized along the x axis, thereby producing alignment in the excited ^1P state relative to the z axis. The helium buffer gas pressure is sufficiently low to avoid significant collisional relaxation of the excited-state coherences. The atomic barium density is kept low to avoid radiation trapping of the 350 nm fluorescence.

The excited atoms are exposed to a uniform, static magnetic field in the positive z direction. The magnetic field was calibrated in a previous experiment [24] to an accuracy of 1%. In the first part of the experiment, a portion of the 532 nm pump beam is directed through the oven to produce the dynamic Stark shift. The 532 nm light is also linearly polarized in the x direction. In the second part, the 532 nm beam is replaced by the output of a second dye laser.

To monitor the orientation of the excited atoms, we detect the intensity of circularly polarized 350 nm fluorescence emitted along the z axis (parallel to the static magnetic field). Two photomultiplier tube detectors with appropriate polarizers and 350 nm filters are used, one to monitor left-circularly-polarized light, the other for right-circular polarization. Gated integrators average the signal over a time long compared to the fluorescence lifetime of the excited state. A computer controls the applied magnetic field, averages the signal from 100 successive pulses, and calculates the circular polarization asymmetry. By taking the difference in the circular polarization asymmetry with the 532 nm beam present and with it absent, we can isolate the 532 nm dynamic Stark shift alignment-to-orientation conversion from other orientation-producing effects. The relative timing of the 350 nm excitation pulse and the 532 nm Stark shift pulse is carefully monitored with a fast p-i-n photodiode detector and a high-speed oscilloscope.

The photomultiplier tubes are surrounded by magnetic shields to reduce the effect of the applied magnetic field on the gain of the tubes. The circular polarizers were measured to have a 90% efficiency in discriminating left-circular polarization from right-circular polarization.

The Stark shift beam is expanded to a diameter of about 2 cm, and the central portion of the beam is selected by a 0.26-cm-diameter pinhole to overlap the 350 nm excitation beam in the center of the oven. By this means we achieve a rough approximation to a uniform intensity of the Stark shift beam over the excited-atom region in the oven since the excitation beam diameter is about 0.1 cm. The average power of the Stark shift beam is measured with a calibrated power meter. Combining the measured average power with

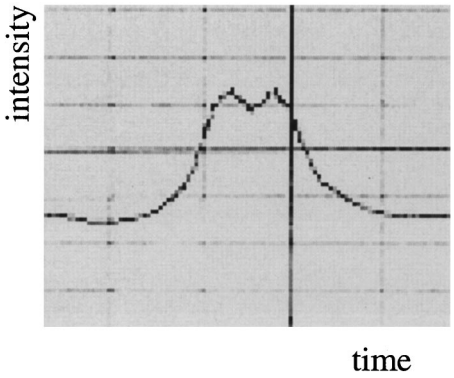

FIG. 6. The temporal profile of the 532 nm Stark shift pulse averaged over 100 consecutive pulses. The time scale is 5 ns per division.

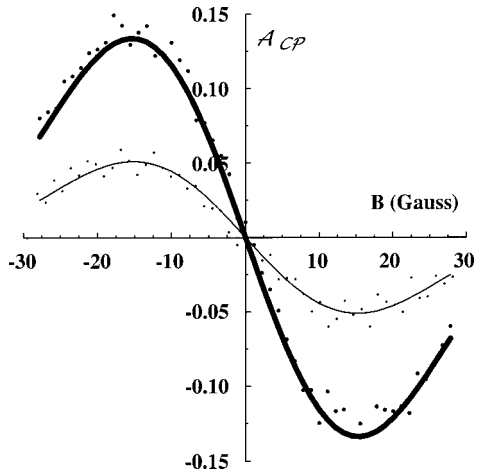

FIG. 7. The circular polarization asymmetry ($\mathcal{A}_{\mathrm{CP}}$) plotted as a function of magnetic field for two different Stark pulse fluences. The dots are the experimental data. The solid curves are the results of a nonlinear least-squares fit to the data. The parameter $p_{\max}$ is the only adjustable parameter. The Stark pulse fluences were 52 J/m^2 (corresponding to $p_{\max}=-0.075$) for the thicker curve and 20 J/m^2 ($p_{\max}=-0.028$) for the thinner curve.

knowledge of the pulse temporal profile and the pulse repetition rate, we can model the overall temporal envelope of the Stark shift electric field.

The time dependence of the electric-field amplitude in the Stark shift beam is relatively complicated with substantial pulse-to-pulse variation due to mode beating in the Nd:YAG laser. The energy per pulse fluctuates by about 3%, but the temporal profile shows much larger variations. Figure 6 shows the 532 nm laser intensity averaged over 100 pulses. The full width at half maximum is about 6 ns. We have modeled the pulse shape in a variety of ways and have found that the integrated circular polarization asymmetry signal is not very sensitive to the details of the pulse shape. Most of the data analysis was carried out with an envelope consisting of the sum of two Gaussian pulses with pulse widths and relative delay chosen to reproduce the pulse shape observed in Fig. 6. The 350 nm excitation pulse was modeled as a half-period sine wave with a half period of 3 ns. Other reasonably realistic excitation pulse shapes gave essentially identical results.

The 532 nm photons are sufficiently energetic to ionize Ba atoms in the $(5d6p)\ ^1P$ state. However, there was no observable change in the intensity of the 350 nm fluorescence signal with the 532 nm laser beam present at the power levels used in this experiment. We conclude that ionization was not significant under our experimental conditions.

IV. EXPERIMENTAL RESULTS

Figure 7 shows the results of two experimental runs along with the results of a nonlinear least-squares fit of the theory to the data. The time-integrated circular polarization asymmetry ($\mathcal{A}_{\mathrm{CP}}$) is plotted as a function of the static magnetic field strength. The relative timing of the excitation and Stark pulse is shown in the upper part of Fig. 3. Since the 350 nm excitation pulse itself also produces a small $\mathcal{A}_{\mathrm{CP}}$, the plotted signal is obtained from the difference in $\mathcal{A}_{\mathrm{CP}}$ with the 532 nm Stark pulse present compared to the $\mathcal{A}_{\mathrm{CP}}$ observed without that pulse. (For the conditions of our experiment, the $\mathcal{A}_{\mathrm{CP}}$ produced by the 350 nm pulse is typically less than 1% and depends sensitively on the detuning from exact resonance.) As expected, $\mathcal{A}_{\mathrm{CP}}$ changes sign when the magnetic field changes sign and the magnitude of the maximum $\mathcal{A}_{\mathrm{CP}}$ increases with increasing energy irradiance of the Stark pulse. (The energy irradiance, that is, the pulse energy per unit area, is also called the fluence.) Since the only adjustable parameter is the tensor polarizability of the excited state, we are able to extract a value for $\alpha_2(\omega)$.

The solid curves in Fig. 7 are the results of a nonlinear least-squares fit of the calculated signal, corrected for the 90% efficiency of the circular polarizers. Averaging the results from five different runs at a variety of Stark pulse fluences, we find that the tensor polarizability of the $(5d6p)\ ^1P$ state is $\alpha_2(\omega=2\pi\ 5.62\times10^{14}\ \mathrm{Hz})=-8.8(7)\times10^{-3}\ \mathrm{MHz/(kV/cm)^2}$, which is opposite in sign and considerably smaller than the static field tensor polarizability $\alpha_2(\omega=0)=+1.31(15)\ \mathrm{MHz/(kV/cm)^2}$ for the same state [24,45]. The experimental uncertainty is determined by combining in quadrature the uncertainties in α_2 due to the least-squares fit ($\pm1\%$), the calibration of the polarizer efficiency ($\pm3\%$), the residual collisional depolarization ($\pm3\%$), and the pulse-to-pulse variations in the energy of the Stark pulses ($\pm7\%$) to obtain the overall experimental uncertainty.

We have used the few known values of transition probabilities for transitions to the $(5d6p)\ ^1P$ state [46] to calculate the reduced matrix elements required in Eq. (4) and extrapolated to other states using the standard $1/n^3$ scaling for the square of the reduced matrix elements to provide a rough estimate of the expected value of the frequency-dependent tensor polarizability. We have not included any continuum contribution. The resulting value for the tensor polarizability at the frequency corresponding to the 532 nm Stark shift beam is $-3.3\times10^{-3}\ \mathrm{MHz/(kV/cm)^2}$, in reasonable agreement with our experimental result, given the crudeness of the estimate.

The calculations described in Sec. II indicate that the atomic orientation should depend sensitively on the timing of

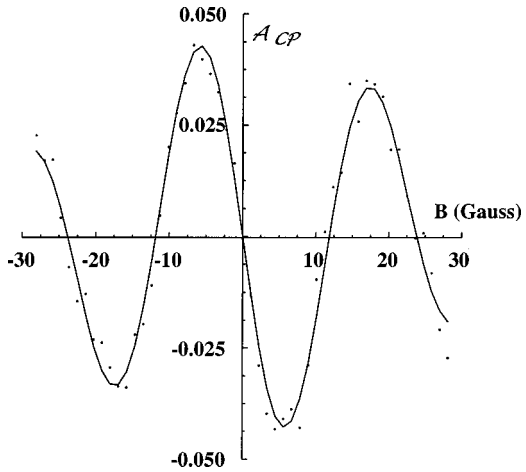

FIG. 8. Circular polarization asymmetry ($\mathcal{A}_{\mathrm{CP}}$) as a function of magnetic field with an additional time delay of 10 ns between the excitation pulse and the Stark pulse as illustrated in the upper part of Fig. 5. The dots are the experimental data. The solid curve is the result of a nonlinear least-squares fit to the experimental data. The Stark pulse fluence is 44 J/m^2.

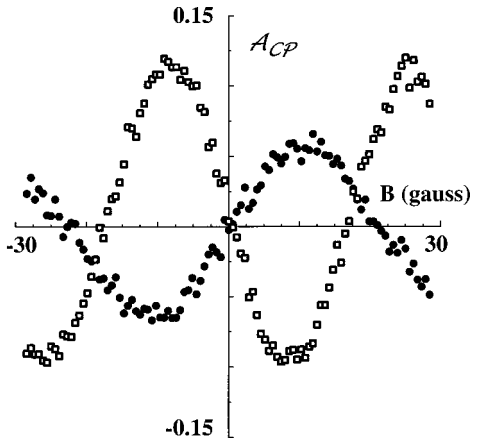

FIG. 9. The time-integrated circular polarization asymmetry ($\mathcal{A}_{\mathrm{CP}}$) plotted as a function of magnetic field. The Stark pulse is provided by a dye laser tuned near 583 nm. The open squares correspond to tuning the dye laser frequency just above the resonance frequency with a nominal detuning of 475 GHz (corresponding to a wavelength detuning of about 0.54 nm). The solid circles correspond to tuning just below the resonance frequency by about 651 GHz.

the excitation pulse and the Stark shift pulse. The data shown in Fig. 7 were taken with approximately 2.4 ns overlap between the end of the excitation pulse and the beginning of the Stark shift pulse as illustrated in Fig. 3. Qualitatively, the shape of the integrated signal as a function of magnetic field is quite similar to the signals observed for static fields [24]. Figure 8 shows the experimental results obtained with an additional delay of 10 ns between the two pulses as shown in the upper part of Fig. 5. With the longer time delay, additional oscillatory structure appears in the signal. In fact, the circular polarization asymmetry can change sign as the magnitude of B increases—an effect that does not occur for static fields.

This behavior can be understood in terms of a classical model [29] of precessing angular momentum vectors, initially developed to explain the static field alignment-to-orientation conversion. According to this model, an atom's angular momentum precesses under the combined influence of a magnetic torque $\vec{\mu}\times\vec{B}$ and an electric torque $\vec{p}\times\vec{E}$, where $\vec{p}$ is the induced electric dipole moment. In this model the initial quantum state is represented by an ensemble of angular momentum vectors distributed uniformly in the yz plane for the conditions of this experiment. If there is a significant delay between the excitation pulse and the Stark shift pulse, the static magnetic field can rotate the ensemble out of the yz plane before the electric field begins its contribution to the precession. For small magnetic-field strengths, there is little rotation and the angular momentum vectors precess under the action of the electric field toward, say, $-z$. For larger values of the magnetic field, the alignment rotates sufficiently that the electric field torque drives the precession toward $+z$. Depending on the precession induced by the magnetic field, which depends on both the strength of the magnetic field and the time delay between excitation and the Stark pulse, the electric-field precession can lead to a net time-integrated orientation along either $+z$ or $-z$.

To provide a further test of the frequency dependence of the tensor polarizability, we replaced the 532 nm Stark shift beam with the output from a tunable dye laser operating near 583 nm, almost in resonance with the $(5d6p)\ ^1P_1-(6s5d)\ 5^1D_2$ transition. As Eq. (4) indicates, the tensor polarizability should increase significantly in magnitude as the frequency of the Stark shift beam approaches the resonant frequency and, in fact, should change sign depending on the sign of the detuning from resonance. Figure 9 shows data taken with the dye laser tuned just above and just below the resonant frequency with a time delay of about 3 ns between the end of the excitation pulse and the beginning of the Stark pulse. The dye laser fluence was approximately 4 J/m^2, substantially smaller than the intensities of the 532 nm Stark pulses used in the first part of the experiment. Nevertheless, the circular polarization asymmetry is about the same magnitude due to the enhanced dynamic polarizability with Stark pulse frequencies close to the transition frequency.

The dye laser data are in qualitative agreement with the previous statement, but the quantitative agreement is less satisfactory. The circular polarization asymmetry changes sign for detuning above and below the resonance. As expected from Eq. (4), blue detuning $[\hbar\omega > E(^1P)-E(^1D)]$ yields a negative dynamic polarizability while red detuning gives a positive value. The lack of quantitative agreement is due primarily to the spectral bandwidth of the dye laser used. Its full-width at half-maximum was about 10 GHz, but it had a rather wide bandwidth of low-level emission due to amplified spontaneous emission. As Eq. (4) indicates, even a relatively low intensity close to the resonant frequency will cause a substantial change in the effective value of the tensor polarizability. In addition, light at the resonance wavelength will cause stimulated emission on the $(5d6p)\ ^1P$ to $(6s5d)\ ^1D$ transition. The stimulated emission will quickly

depopulate the ^1P state and hence dramatically reduce any circular polarization asymmetry on the $^1P-{}^1S$ transition at 350 nm. Given these complications, we did not attempt to provide a quantitative fit of the theory to the data.

V. SUMMARY AND CONCLUSIONS

We have shown that the dynamic Stark shift can have a dramatic effect on the coherence properties of atomic excited states. In the presence of a magnetic field orthogonal to the oscillating electric field, the atom can obtain a large degree of orientation from an initially aligned state. The large orientation leads to reasonably sensitive measurements of the frequency-dependent polarizability of the atomic excited state. For a Stark shift optical field nearly in resonance with an atomic transition, the induced orientation changes sign with the detuning from resonance, as expected. We also demonstrated the effects of a time delay between the excitation pulse and the Stark shift light pulse. Although these effects are most easily seen and interpreted in the simple $J=0$ to 1 atomic transition used here, they should appear in almost any atomic transition with an excited state $J\geqslant 1$.

[1] S. H. Autler and C. H. Townes, Phys. Rev. **100**, 703 (1956).
[2] I. I. Sobelman, *Atomic Spectra and Radiative Transitions* (Springer-Verlag, Berlin, 1979).
[3] Y. Zhang, M. Ciocca, L.-W. He, C. E. Burkhardt, and J. J. Levanthal, Phys. Rev. A **50**, 1101 (1994).
[4] M. A. Kadar-Kallen and K. D. Bonin, Phys. Rev. Lett. **72**, 828 (1994).
[5] V. Vuletic and S. Chu, Phys. Rev. Lett. **84**, 3787 (2000).
[6] E. M. Rasel, M. K. Oberthaler, H. Batelaan, J. Schmiedmayer, and A. Zeilinger, Phys. Rev. Lett. **75**, 2633 (1995).
[7] D. M. Giltner, R. W. McGowan, and S. A. Lee, Phys. Rev. Lett. **75**, 2638 (1995).
[8] J. H. Eberly and K. C. Kulander, Science **262**, 1229 (1993).
[9] M. Brune, S. Haroche, V. Lefevre, J. M. Raimond, and N. Zagury, Phys. Rev. Lett. **65**, 976 (1990).
[10] M. Brune, S. Haroche, J. M. Raimond, L. Davidovich, and N. Zagury, Phys. Rev. A **45**, 5193 (1992).
[11] B. S. Mathur, H. Tang, and W. Happer, Phys. Rev. **171**, 11 (1968).
[12] B. Friedrich and D. Herschbach, Phys. Rev. Lett. **74**, 4623 (1995).
[13] L. Cai, J. Marango, and B. Friedrich, Phys. Rev. Lett. **86**, 775 (2001).
[14] R. N. Zare, *Angular Momentum* (Wiley, New York, 1988).
[15] K. Blum, *Density Matrix Theory and Applications*, 2nd ed. (Plenum, New York, 1996).
[16] U. Fano and J. H. Macek, Rev. Mod. Phys. **45**, 553 (1973).
[17] A. C. Kunmel, G. O. Sitz, and R. N. Zare, J. Chem. Phys. **88**, 7357 (1988).
[18] N. Andersen, in *Atomic, Molecular, & Optical Physics Handbook*, edited by G. Drake (AIP, Woodbury, NY, 1996), p. 526.
[19] E. D. Commins, Am. J. Phys. **61**, 778 (1993).
[20] M. Lombardi, J. Phys. (Paris) **30**, 631 (1969).
[21] C. Cohen-Tannoudji and J. Dupont-Roc, Opt. Commun. **1**, 184 (1969).
[22] C. Cohen-Tannoudji and J. Dupont-Roc, Phys. Rev. A **5**, 968 (1972).
[23] M. P. Auzinsh, Phys. Lett. A **169**, 463 (1992).
[24] R. C. Hilborn, L. R. Hunter, K. Johnson, S. K. Peck, A. Spencer, and J. Watson, Phys. Rev. A **50**, 2467 (1994).
[25] D. Budker, D. F. Kimball, S. M. Rochester, and V. V. Yashchuk, Phys. Rev. Lett. **85**, 2088 (2000).
[26] M. P. Auzinsh and R. S. Ferber, J. Chem. Phys. **99**, 5742 (1993).
[27] I. Lincare, M. Tamanis, A. Stolyarov, M. Auzinsh, and R. Ferber, J. Chem. Phys. **99**, 5748 (1993).
[28] J. v. Milczewski, G. H. F. Dierchksen, and T. Uzer, Phys. Rev. Lett. **73**, 2428 (1994).
[29] R. C. Hilborn, Am. J. Phys. **63**, 330 (1995).
[30] J. A. Gupta, R. Knobel, N. Samarth, and D. D. Awschalom, Science **292**, 2458 (2001).
[31] A. M. Bonch-Bruevich and V. A. Khodovoi, Sov. Phys. Usp. **10**, 637 (1967).
[32] N. L. Manakov, V. D. Ovsiannikov, and L. P. Rapoport, Phys. Rep. **141**, 319 (1986).
[33] J. R. P. Angel and P. G. H. Sandars, Proc. R. Soc. London, Ser. A **305**, 125 (1968).
[34] A. Khadjavi, A. Lurio, and W. Happer, Phys. Rev. **167**, 128 (1968).
[35] L. O. Dickie and F. M. Kelly, Can. J. Phys. **49**, 2630 (1971).
[36] U. Fano, Phys. Rev. **133**, B828 (1964).
[37] M. P. Auzinsh and R. S. Ferber, Phys. Rev. A **43**, 2374 (1991).
[38] M. Auzinsh and R. Ferber, *Optical Polarization of Molecules* (Cambridge University Press, Cambridge, England, 1995).
[39] V. Milner and Y. Prior, Phys. Rev. A **59**, R1738 (1999).
[40] V. Milner, B. M. Chernobrod, and Y. Prior, Phys. Rev. A **60**, 1293 (1999).
[41] S. M. Rochester and D. Budker, Am. J. Phys. **69**, 450 (2001).
[42] F. T. Arecchi, E. Courtens, R. Gilmore, and H. Thomas, Phys. Rev. A **6**, 2211 (1972).
[43] G. S. Agarwal, Phys. Rev. A **24**, 2889 (1981).
[44] X. L. Han and G. W. Schinn, Phys. Rev. A **43**, 266 (1991).
[45] K. A. H. van Leeuwen and W. Hogervorst, Z. Phys. A **310**, 37 (1983).
[46] *CRC Handbook of Chemistry and Physics*, edited by D. R. Lide (CRC Press, Boca Raton, FL, 1996).